Communications in Physics, Vol. 32, No. 4 (2022), pp. 423-436
DOI: https://doi.org/10.15625/0868-3166/16674

OPTO-ELECTRONIC PROPERTIES OF SMALL ZnO_2 NANOPARTICLES: FIRST-PRINCIPLES INSIGHTS

DANG MINH TRIET[1], PHAM THI BICH THAO[2] AND NGUYEN THANH TIEN[2,†]

[1]*School of Education, Can Tho University, 3-2 Road, Can Tho City 900000, Vietnam*
[2]*College of Natural Sciences, Can Tho University, 3-2 Road, Can Tho City 900000, Vietnam*

E-mail: [†]nttien@ctu.edu.vn

Received 31 October 2021
Accepted for publication 20 June 2022
Published 5 September 2022

Abstract. *We performed density functional theory based first-principles calculations to investigate the opto-electronic properties of small ZnO_2 nanoparticles. We have shown that these ZnO_2 nanoparticles can exhibit either semiconductor or metallic properties depending on the morphology and sizes of the nanoparticles defined by Miller indices. The absorption spectra computed from the real and imaginary parts of the dielectric functions demonstrate that these nanoparticles exhibit rich optical features with highly spatial anisotropy in the visible light range, suggesting that these newly obtained configurations strongly influence the electronic structures of ZnO_2 nanoparticles. Our results propose the potential application of using Zinc peroxide nanoparicles as prospective building blocks for developing early diagnosis nanodevices in drug industry.*

Keywords: density functional theory, opto-electronic properties, Zinc peroxide, nanoparticles.

Classification numbers: 31.15.E; 42.82.Fv.

I. INTRODUCTION

Nano-scale materials, a rich class of nano-particles, nano-wires, nanoribbons, thin films, and component structures, have received a vast attention from both theoretical and experimental physicists since the discovery of fullerenes and the emergence of carbon nanotubes in the 1990s [1–6]. Among these types of nano-scale materials, nano-particles have been strongly investigated in multidisplinary industries, including medicine, cosmetics, materials, energy and environment [7–13]. Nano-particles with a size of smaller than 100 nm existing in multiple structures varying from zero to three-dimensions [14, 15] are the core strategy to improve the bioavailability, substance stability and safety of the next generation of drug technology [16, 17]. It is because these nanoparticles, thanks to their small sizes, large surface free energies and large contact areas, can significantly magnify the dissolution rate, thereby increase the bioavailability of drugs in living organisms. Furthermore, under the same activation conditions, some targeted nanoparticles sufficiently reinforce the absorption efficiency of drugs via their ability to shine 20 times brighter and maintain the brightness coefficient much longer than fluorescent molecules [16]. The ultimate combination of highly mobile and long-lived photoluminescence of targeted nano-particles allows physicians to follow living cells deep inside the body with better image contrast, and so as undoubtedly useful for early diagnosis [18].

Among the class of nano-scale materials, recently, TiO_2, ZnO, and ZnO_2 have been shown as excellent candidates for their potential applications in photocatalytics [19], gas sensing [20], photovoltaics [21] and especially in pharmaceutical technology thanks to their antibacterial efficacies [22, 23].

More interestingly, ZnO_2 (Zinc peroxide), a novel material with rich morphological configurations, promises great applications in (pharmaceutical-) industry. ZnO_2 is thermally stable up to 250 ^{0}C and can be created in vast of synthesized methods [24–28]. Also, ZnO_2 can be hydrothermalized from a sol-gel phase to be used as a precursor to create nanometric ZnO particles [22, 29] and ultrasmall functional ZnO_2 nanoparticles [30].

While detailed studies on the electronic and optical properties of ZnO nanoparticles have been reported tremendously over the last decade, experimental and theoretical research on the opto-electronic properties of ZnO_2 nanoparticles are still limited. Thus, in this paper, we report the electronic and optical properties of small ZnO_2 nanoparticles with different nanoparticle sizes and shapes (crystal growing planes) using density functional theory. We designed six types of nanoparticles including ZnO_2(001)-21, ZnO_2(001)-41, ZnO_2(001)-187, ZnO_2(111)-13, ZnO_2(111)-33 and ZnO_2(111)-173, where (001) and (111) denote the Miller indices while the latter numbers correspond to the number of Zn and O atoms in these nanoparticles, and examined their electronic and optical properties in detail.

II. COMPUTATIONAL METHODS

In this work, we created ZnO_2 nanoparticles according to the Wulff construction with suitable Miller indices and their corresponding minimum surface energies using the novel web-base crystallographic Nano-Crystal tool [31]. Using this tool, we have found the two most stable facet ZnO_2 nanoparticles with their minimum surface energy values of 62 eV for ZnO_2(001) and 35 eV for ZnO_2(111), respectively. We then created six ZnO_2 samples with increasing nanoparticle sizes from a ZnO_2 pyrite crystal as shown in Fig. 1. The ZnO_2 crystallographic file can be downloaded

from Ref. [32]. Six investigated samples include three samples in the (001) Miller plane (namely ZnO_2(001)-21, ZnO_2(001)-41, ZnO_2(001)-187, the latter numbers in each sample names denote the total numbers of atoms in each nanoparticles corresponding to the values of 21, 41 and 187, respectively) and three samples in the (111) Miller plane (namely ZnO_2(111)-13, ZnO_2(111)-33 and ZnO_2(111)-173 with the equivalent numbers of atoms of 13, 33 and 173, respectively).

All opto-electronic properties of ZnO_2 nanoparticles were calculated using the density functional theory (DFT) predictions implemented in the Atomistix Toolkit (ATK) package [33, 34]. For the Generalized Gradient Approximation (GGA), the Perdew–Burke–Ernzerhof (PBE) with a double-ζ polarized basis is applied to handle the exchange-correlation function. Monkhorst–Pack grids of $5\times5\times5$ k-points were used for the geometry optimization, and one k-point (Γ point) for the calculation of optoelectronic properties. The cut-off energy was about 500 eV. Vacuum spaces of at least 15 Å are applied on all three axes of the investigated samples to avoid the interactions between the periodic images. This approach is to ensure the reproducibility and reliability of our opto-electronic calculations for all ZnO_2 nanoparticles.

The optical properties of materials were determined by a complex dielectric function [35, 36]:

$$\varepsilon(\omega)=\varepsilon_1(\omega)+i\varepsilon_2(\omega). \tag{1}$$

Here, $\varepsilon_1(\omega)$ and $\varepsilon_2(\omega)$ are the real part and the imaginary part of the dielectric function, respectively. The dielectric function is related to the susceptibility as

$$\varepsilon(\omega)=1+\chi(\omega). \tag{2}$$

where ω indicates the angular frequency of the incident photon. $\chi(\omega)$ is calculated by the Kubo-Greenwood formula [37]. From here, we can determine the extinction coefficient κ, and the optical absorption coefficient α of the materials as follows [35, 38]:

$$\kappa=\sqrt{\frac{\sqrt{\varepsilon_1^2+\varepsilon_2^2}}{2}-\frac{\varepsilon_1}{2}}, \tag{3}$$

$$\alpha=\frac{2.\omega}{c}\kappa, \tag{4}$$

where c is the velocity of light in vacuum. Note that we use the independent particle approximation for linear optical response functions to establish a link between the electronic band structures and the optical properties of the nanoparticles.

III. RESULTS AND DISCUSSION

III.1. Structural properties

Figure 1 and Table 1 present the most energetically favorable ZnO_2 nanoparticle configurations and their size parameters in the edges and the diagonal directions. The distances d_1, d_2 represent for the sizes of the cubic nanoparticles in the edge and the diagonal directions before DFT optimization while d_1', d_2' are those equivalent lengths after optimization. It is obvious that after optimization, the nanoparticles rearrange in such a way to increase the compactness of the particles resulting in the decrease of d_1', d_2' with respect to d_1, d_2 distances.

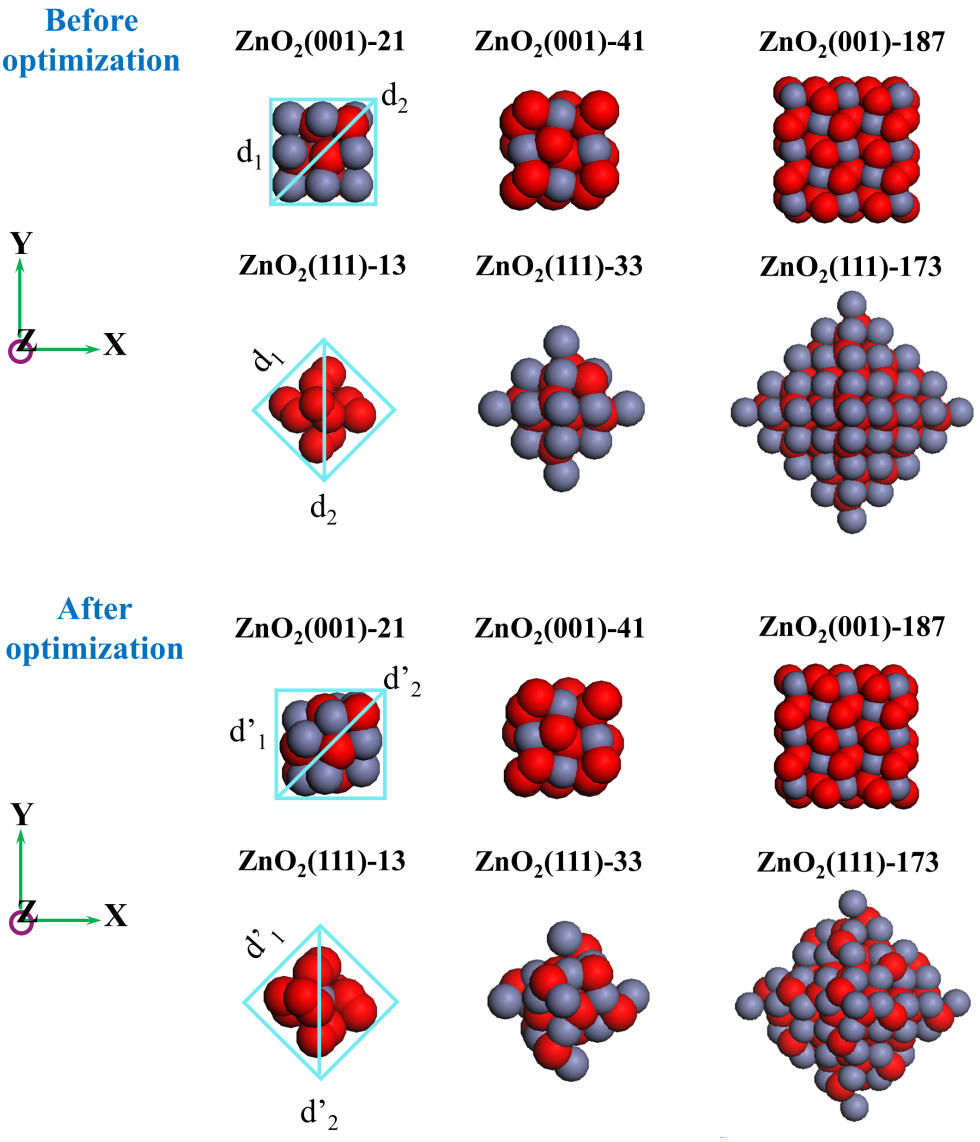

Fig. 1. Configurations of ZnO_2 nanoparticles before and after optimization with different numbers of atoms. Gray and red balls represent for Zinc and Oxygen atoms, respectively.

To confirm that these acquired nanoparticles are the most stable configurations, we calculate their binding energies as following:

$$E_B = \frac{E_{ZnO_2} - n_{Zn}E_{Zn} - n_O E_O}{n_{Zn} + n_O}. \tag{5}$$

Here, E_{ZnO_2} is the total energy of ZnO_2 nanoparticles, E_{Zn}, E_O are the energies of the isolated Zinc and Oxygen atoms, and n_{Zn}, n_O are the atom numbers of Zinc and Oxygen atoms, respectively.

Table 1. Size parameters in the edges and diagonal directions of the ZnO_2 nanoparticles before and after geometrical optimization.

Samples	d_1 (Å)	d_1' (Å)	d_2 (Å)	d_2' (Å)
ZnO_2(001)-21	4.90	4.20	6.93	5.90
ZnO_2(001)-41	4.96	4.80	7.01	6.74
ZnO_2(001)-187	9.92	9.41	14.02	13.30
ZnO_2(111)-13	4.21	3.96	5.95	5.68
ZnO_2(111)-33	7.01	6.63	9.92	9.45
ZnO_2(111)-173	14.02	14.01	19.83	19.83

Table 2. Binding energy of ZnO_2 nanoparticles.

Samples	Zn atoms	O atoms	Binding energy, E_B (eV)
ZnO_2(001)-21	13	8	-2.6
ZnO_2(001)-41	13	28	-3.7
ZnO_2(001)-187	63	124	-3.9
ZnO_2(111)-13	1	12	-4.1
ZnO_2(111)-33	19	14	-3.1
ZnO_2(111)-173	85	88	-2.9

Table 2 shows the binding energies of two groups of ZnO_2(001) and ZnO_2(111) nanoparticles. The calculated binding energy varying in between -2.6 eV and -4.1 eV demonstrates that these investigated nanoparticles are stabilized. For the ZnO_2(001) nanoparticles, their binding energies decrease with increasing particle sizes, suggesting that the larger ZnO_2 nanoparticles are more stable than the smaller ones. However, for ZnO_2(111) nanoparticles, this quantity increases when increasing the nanoparticle sizes, pointing out that larger ZnO_2(111) nanoparticles may be less stable.

III.2. Electronic properties

We now turn our attention to the electronic properties of the optimized ZnO_2 nanoparticles. Figs. 2 and 3 present the calculated band structures and the corresponding density of states of all investigated nanoparticles. For the sake of comparison, we set the Fermi level to zero and only plotted the calculated energy levels 2 eV around the Fermi level. In Fig. 2, it is obvious that ZnO_2 nanoparticles exhibit semiconductor behavior with a bandgap of ~ 0.3 eV for both ZnO_2(001)-21 and ZnO_2(111)-13, while the rest of the investigated samples are electrically metallic. Here, we defined the energy band gap as the energy difference between the highest occupied molecular

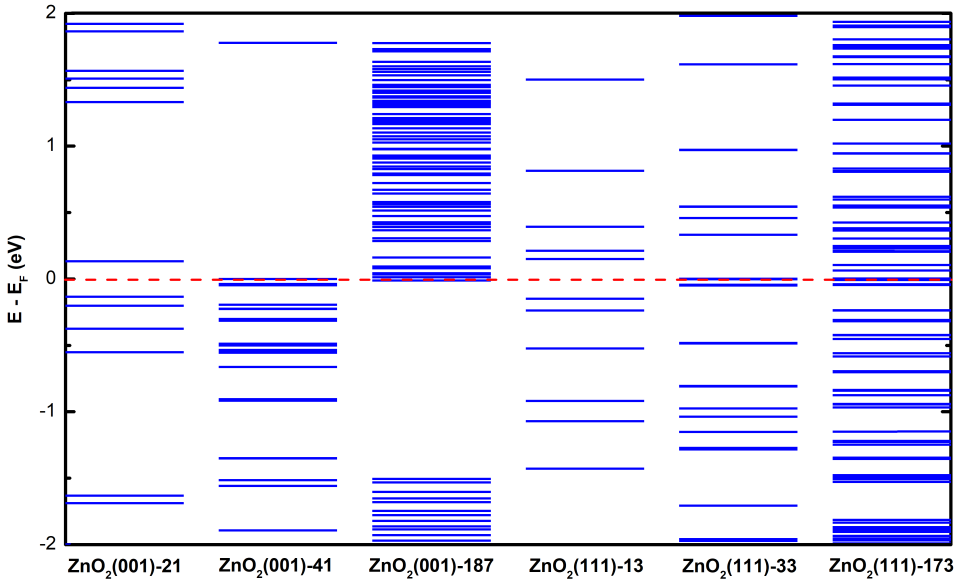

Fig. 2. Energy levels of ZnO_2 nanoparticles, for different sizes and configurations. The dashed lines indicate the Fermi level.

orbitals (HOMO) and the lowest unoccupied molecular orbitals (LUMO). This band structure explicitly indicates that the energy band gaps of the nanoparticles significantly shrink and even vanish when these nanoparticles are big in their atom sizes, pointing out a distinct difference between these nanoparticles and the ZnO_2 pyrite crystal. Note that the band gap of ZnO_2 pyrite crystal is 2.2 eV [32]. Thus, the morphology of the ZnO nanoparticles is central to control the electronic properties of these interesting nanoparticles.

To understand this striking observation, we further explore the role of each type of atoms on the partial density of states in Fig. 3. In the case of ZnO_2 pyrite crystal, Oxygen atoms are the major contributor to both conduction and valence states [32]. However, for ZnO_2(001)-41, ZnO_2(001)-187 and ZnO_2(111)-13, the valence band states are mainly contributed by Oxygen atoms while for the other nanoparticles, Zinc atoms seem to dominate. In the conduction bands, for ZnO_2(001)-21, ZnO_2(001)-41, ZnO_2(111)-33 and ZnO_2(111)-173, Zinc atoms play a predominant role. An opposite trend was observed for ZnO_2(001)-187 and ZnO_2(111)-13. In short, the contribution of Zinc and Oxygen atoms to the density of states varies depending on the surface morphology of certain nanoparticles.

III.3. Optical properties

In this section, we present the optical properties of ZnO_2 nanoparticles. These properties, which are closely related to their electronic band structures, indicate the possibility for using this class of materials for early diagnosis nano-devices in drug industry. To examine the absorption capacity of these nanoparticles, we first calculate the real and imaginary parts of the optical dielectric response functions, and then determine the absorption coefficient ($\alpha(\omega)$) using the equations presented in Sec. II. In these calculations, we have chosen the polarization direction parallel to the electric field.

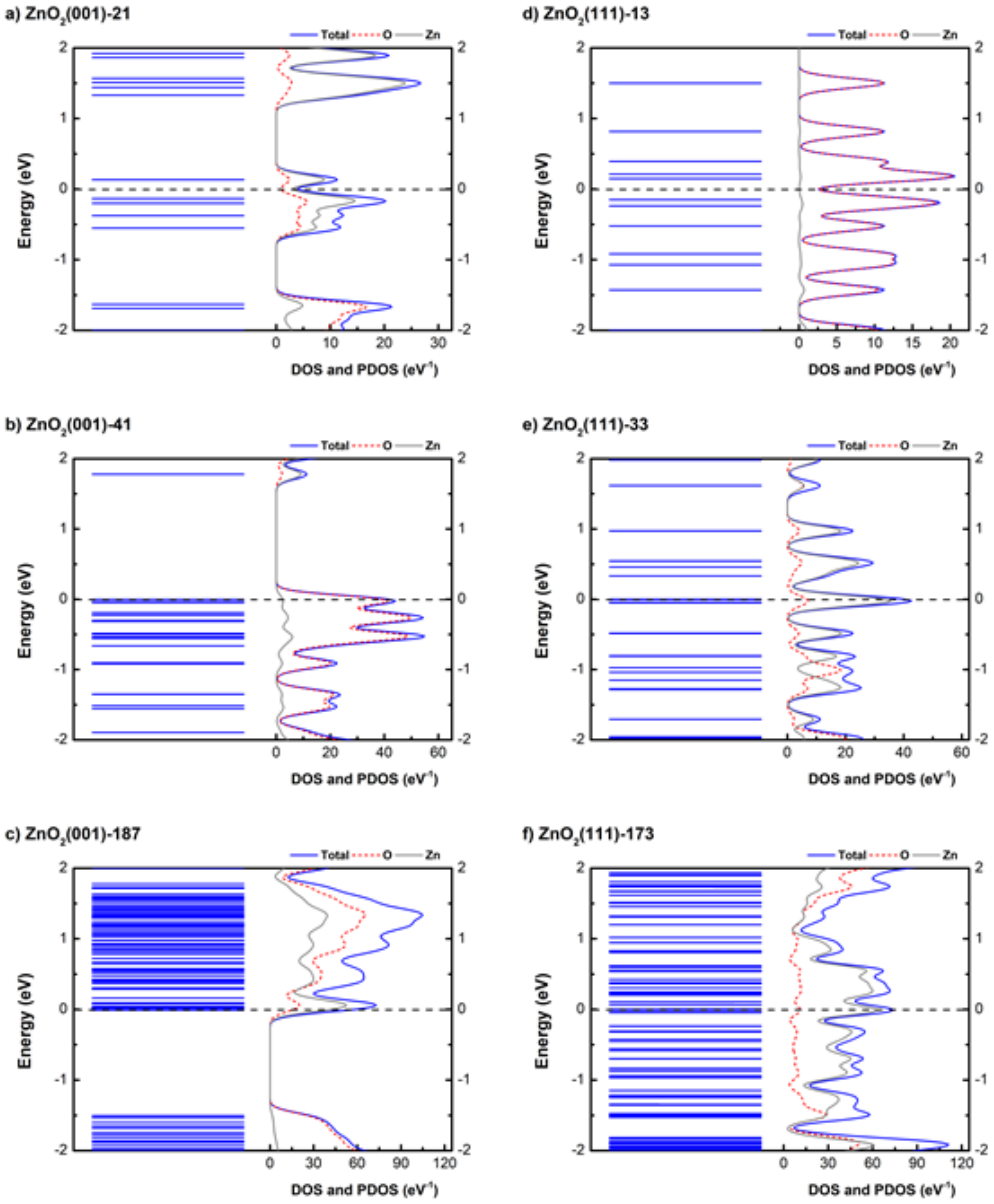

Fig. 3. DOS and PDOS of the ZnO_2 nanoparticles. The dashed lines indicate the Fermi level. Electronic band structure is also included for ease of analysis

The electronic polarizability indicating the absorption capacity of the material can be determined from the real and imaginary parts of the dielectric functions. In Fig. 4, we show the real parts of the dielectric functions of all investigated samples as a function of the incident photon energy. It is clear that for nanoparticles with the number of atoms above 33, the real parts of the dielectric functions do not show a significant difference in all three polarizations. However, for the

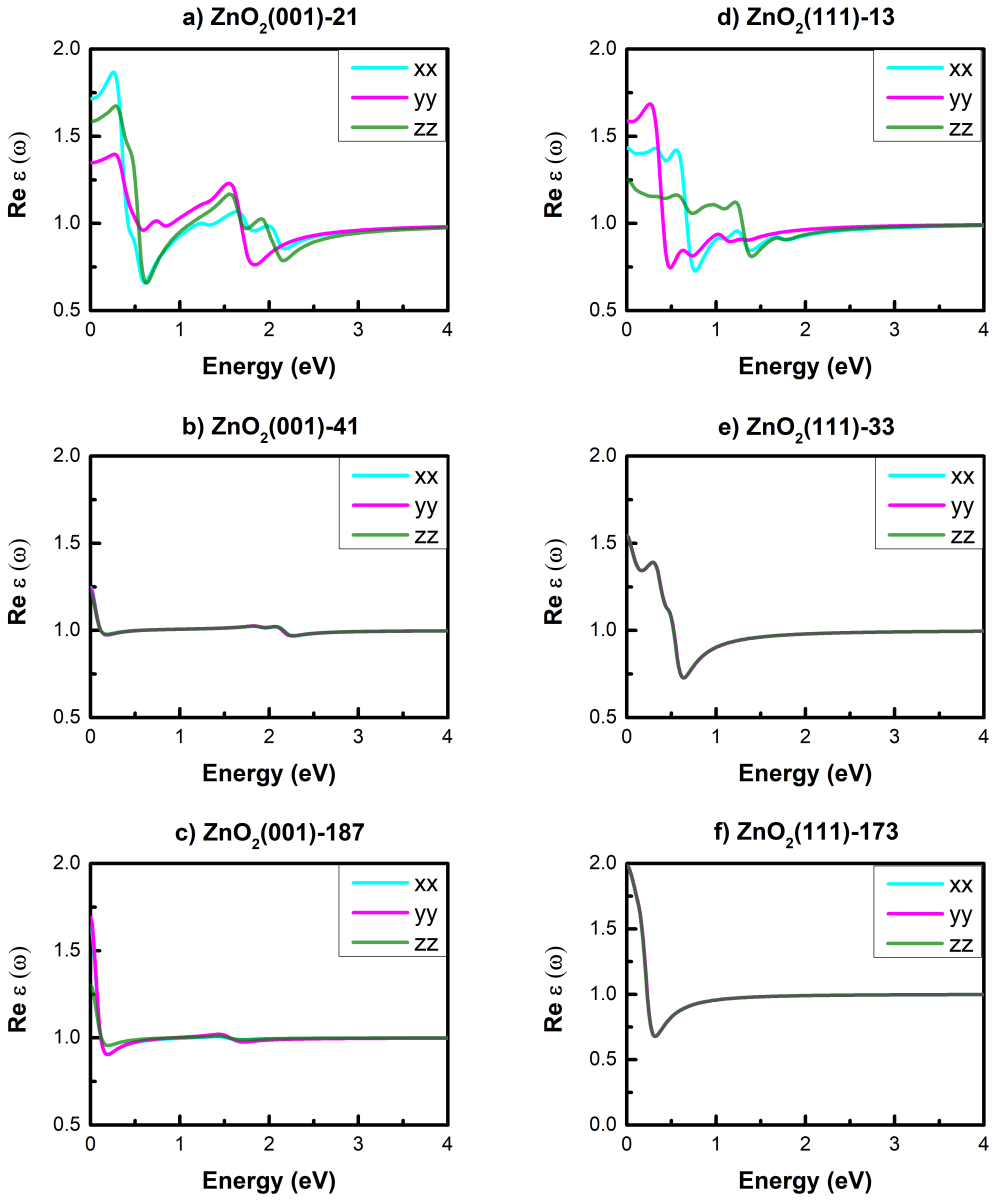

Fig. 4. Real part of the dielectric funtion of the ZnO_2 nanoparticles.

two smallest nanoparticles (ZnO_2(001)-21 and ZnO_2(111)-13 samples), we observe a noticeable spatial anisotropy of the real parts in the low energy range. Specifically, the maximum value of $\varepsilon_1(\omega)$ for ZnO_2(001)-21 nanoparticles is approximately 2 in the x direction, while this value in the y direction is below 1.5. For ZnO_2(111)-13 nanoparticles, the dominant peak of $\varepsilon_1(\omega)$ is about 1.75 in the y direction. In the visible light range (the incident photon energy is in between 1.65

eV and 3.2 eV), ZnO_2(001)-21 nanoparticles show a better response of $\varepsilon_1(\omega)$ compared to that of ZnO_2(111)-13.

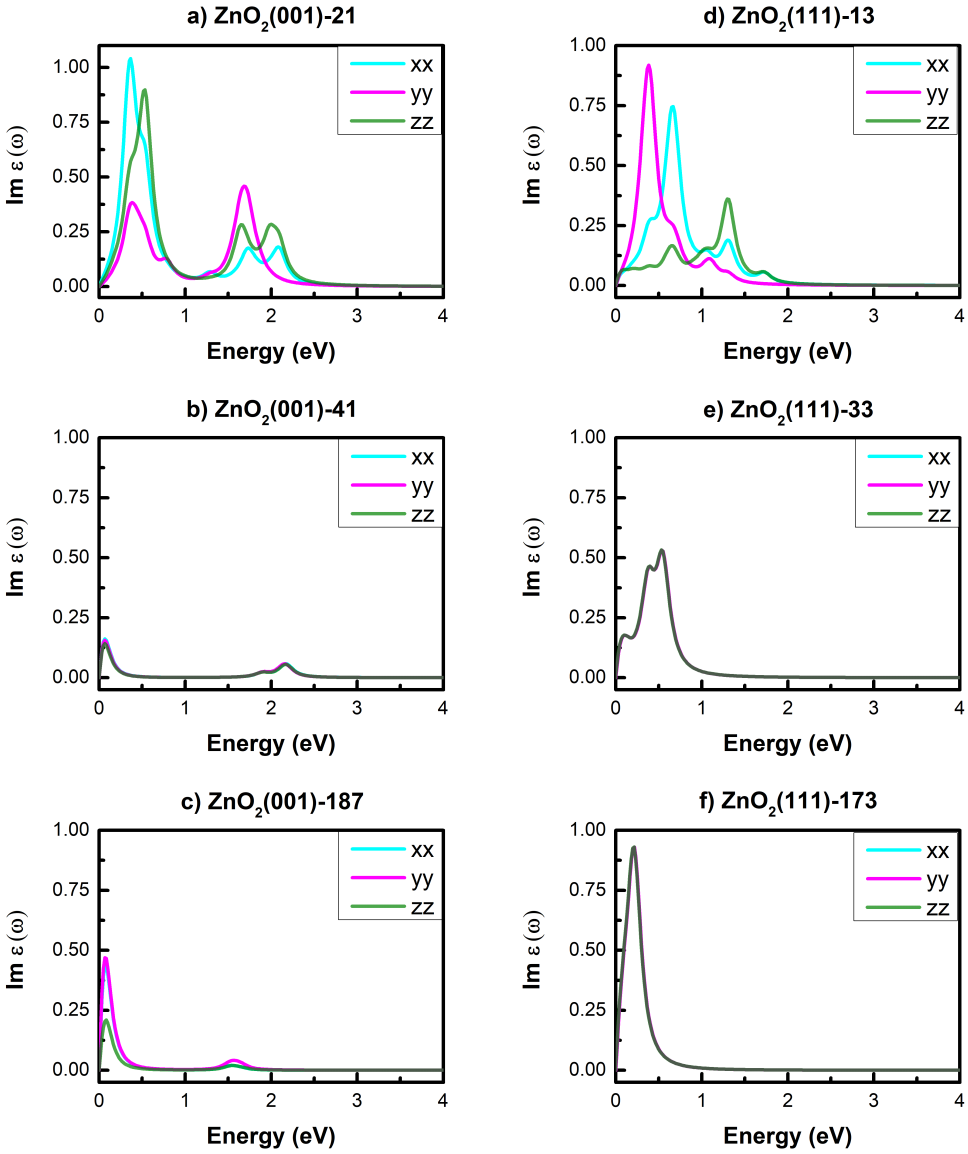

Fig. 5. Imaginary part of the dielectric funtion of the ZnO_2 nanoparticles.

We then show the imaginary parts of the dielectric function $\varepsilon_2(\omega)$ of all ZnO_2 samples in Fig. 5. These calculations share common optical features to the absorption coefficients presented in Fig. 6. Explicitly, the dominant absorption peaks of ZnO_2(111)-33 and ZnO_2(111)-173 appear in the energy range below 1.0 eV (mostly in the infrared region), whereas ZnO_2(001)-21,

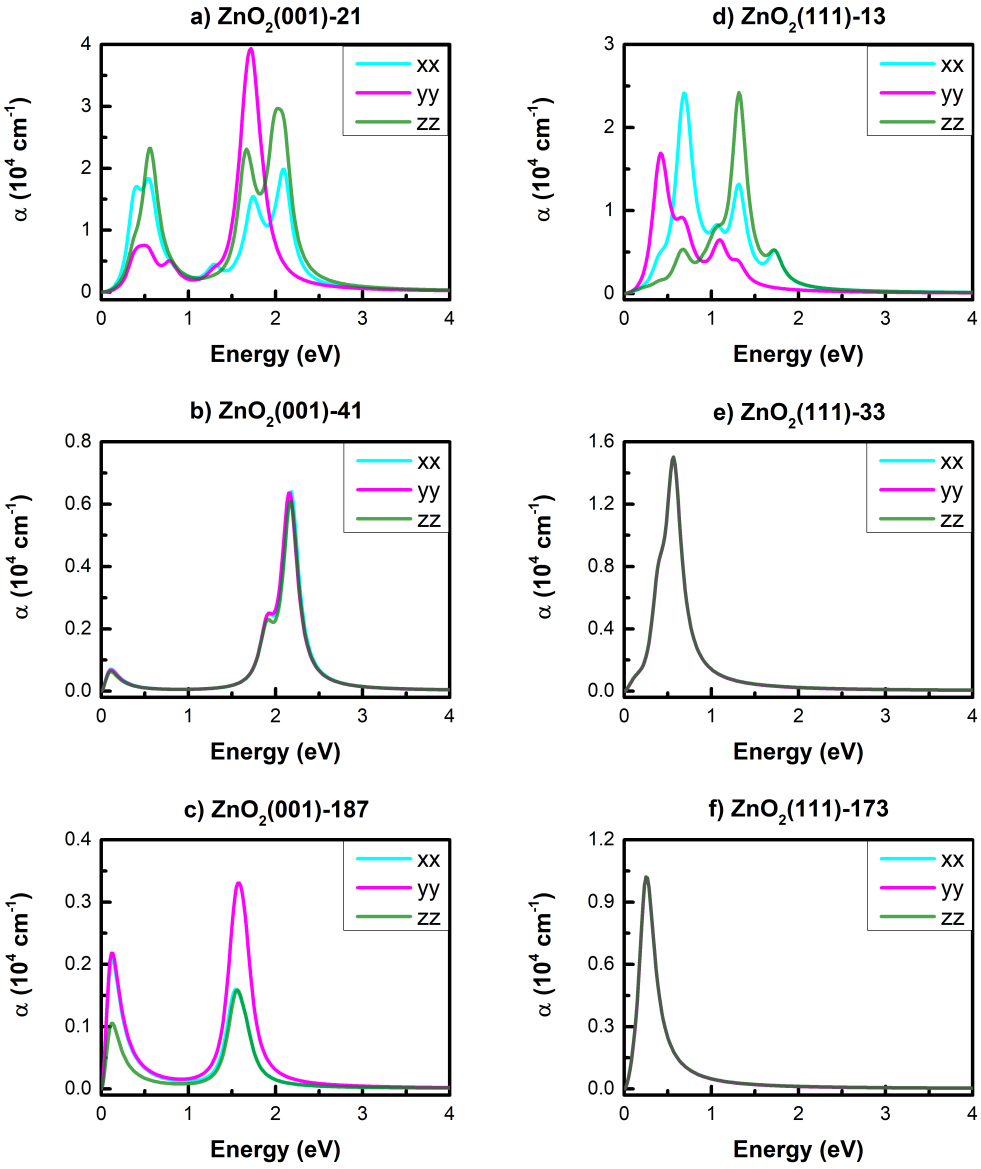

Fig. 6. Spatial anisotropic absorption coefficients of ZnO_2 nanoparticles.

ZnO_2(001)-41, ZnO_2(001)-187 and ZnO_2(111)-13 are more sensitive in the visible range. The imaginary part of the dielectric functions of ZnO_2(001)-21 and ZnO_2(111)-13 is highly asymmetry.

The absorption coefficient as a function of photon energy is calculated and shown in Fig. 6. To quantize the dominant peaks of these spectra with the electronic band structures, we sketch

these transition states in Fig. 7 and Fig. 8. It is well-known that the band-to-band absorption radiation can be generated by the photoexcitation of an electron being excited from a valence band to a conduction band. This transition can be direct or indirect. In the case of ZnO_2 nanoparticles, we associate the absorption coefficient spectra with direct transitions.

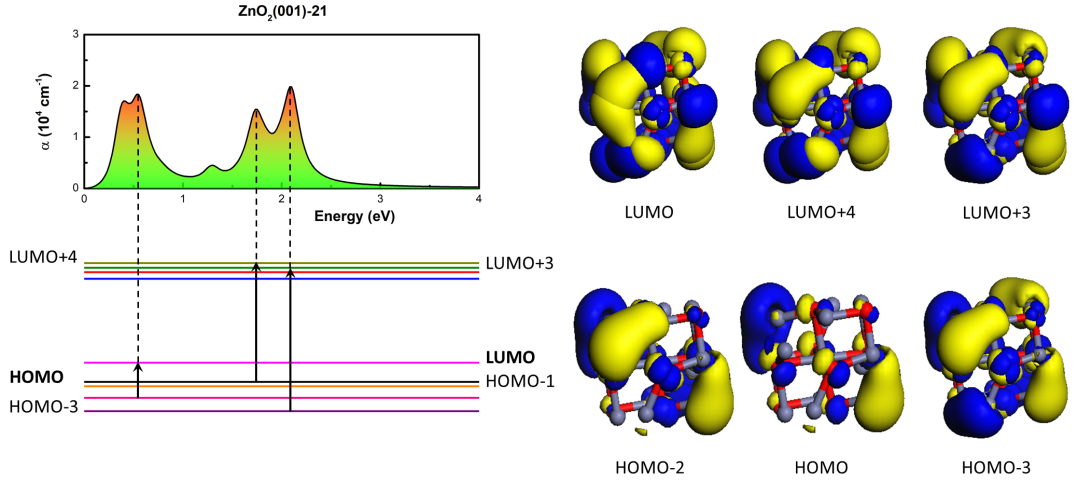

Fig. 7. Left: The electronic transition of states; Right: HOMO and LUMO (The isovalue set is 0.05) of several typical states for ZnO_2(001)-21.

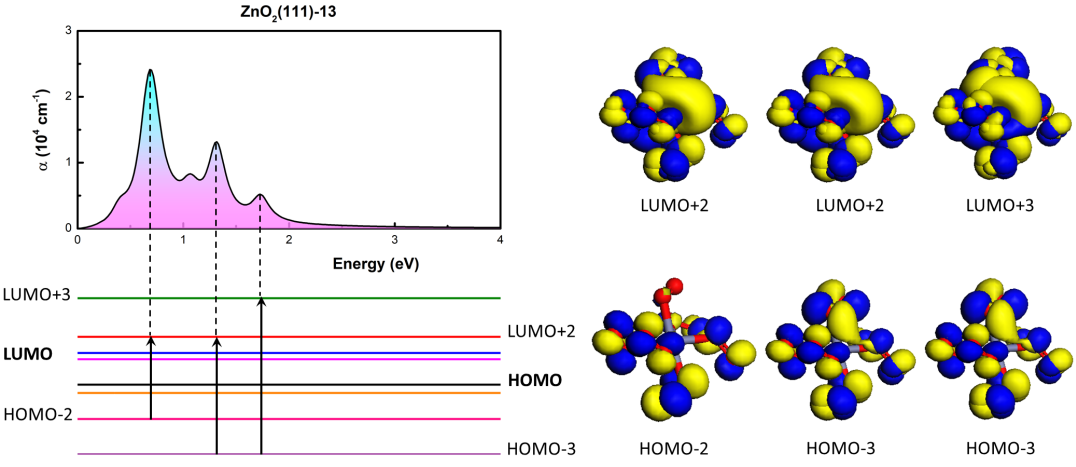

Fig. 8. Left: The electronic transition of states; Right: HOMO and LUMO (The isovalue set is 0.05) of several typical states for ZnO_2(111)-13.

For the case of ZnO_2 nanoparticles, except for ZnO_2(111)-33 and ZnO_2(111)-173 dominant peaks in the infrared region, the remaining nanoparticles exhibit dominant peaks in the visible light range, suggesting promising applications for early medical diagnosis devices. Furthermore, to elucidate the formation of these transition states, we present the band-to-band analyses and plot the highest occupied molecular orbital (HOMO) and the lowest unoccupied molecular orbital (LUMO) configurations of several typical states for two samples ZnO_2(001)-21 and ZnO_2(111)-13 in Fig. 7 and Fig. 8. For ZnO_2(001)-21 nanoparticles, there are the absorption peaks corresponding to electronic transitions: H-3 $\longrightarrow$ L+3, H $\longrightarrow$ L+4, H-2 $\longrightarrow$ L. The strongest peak occurs at an excitation energy of 2.1 eV corresponding to the electronic transition from H-3 $\longrightarrow$ L+3 in ZnO_2(001)-21. Also, the electronic transition from H-2 $\longrightarrow$ L matches the peak of the lowest intensity at 0.53 eV. In the case of ZnO_2(111)-13 nanoparticles, we obtain three peaks equivalent to the electronic transition from H-3$\longrightarrow$ L+3, H-3$\longrightarrow$ L+2 and H-2 $\longrightarrow$ L-1 at energy levels of 1.72, 1.3 and 0.7 eV, respectively. Thus, these results mark the novel optoelectronic properties of small or ultrasmall ZnO_2 nanoparticles. This demonstrates the richness of the optoelectronic properties of the small nanoparticles, which is not observed by ZnO_2 pure crystals [39].

IV. CONCLUSION

In summary, using DFT calculations, we have systematically investigated the opto-electronic properties of small nanoparticles, ZnO_2(001) and ZnO_2(111). By increasing the size and altering the surface orientations of the nanoparticles, we can tune the band gaps as well as the electronic properties of the ZnO_2 nanoparticles. Specifically, the two smallest nanoparticles exhibit semiconductor properties, while the rest of the investigated samples are electrically metal. Furthermore, albeit these nanoparticles are still small in size, we observe noticeable spatial anisotropies of absorption spectra indicating a reconciliation of the nanoparticle morphology and interfacial surface tensions. These results demonstrate the possibility of using ZnO_2 nanoparticles as an excellent candidate for developing the next generation of early diagnosis devices.

ACKNOWLEDGMENT

This research is funded by Vietnam National Foundation for Science and Technology Development (NAFOSTED) under grant number 103.01-2018.308. The authors also would like to express a special thank to the Information and Network Management Center at Can Tho University for the computational support.

REFERENCES

[1] A. Astefanei, O. Núñez and M. T. Galceran, *Characterisation and determination of fullerenes: a critical review*, *Anal. Chim. Acta* **882** (2015) 1.
[2] S. Iijima, *Helical microtubules of graphitic carbon*, *Nature* **354** (1991) 56.
[3] S. Iijima and T. Ichihashi, *Single-shell carbon nanotubes of 1-nm diameter*, *nature* **363** (1993) 603.
[4] N. T. Tien, P. T. B. Thao, V. T. Phuc and R. Ahuja, *Electronic and transport features of sawtooth penta-graphene nanoribbons via substitutional doping*, *Physica E Low Dimens. Syst. Nanostruct.* **114** (2019) 113572.
[5] N. T. Tien, P. T. B. Thao, V. T. Phuc and R. Ahuja, *Influence of edge termination on the electronic and transport properties of sawtooth penta-graphene nanoribbons*, *J. Phys. Chem. Solids* (2020) 109528.
[6] D. K. Nguyen, N. T. T. Tran, T. T. Nguyen and M.-F. Lin, *Diverse electronic and magnetic properties of chlorination-related graphene nanoribbons*, *Sci. Rep.* **8** (2018) 1.

[7] J. E. Lee, N. Lee, T. Kim, J. Kim and T. Hyeon, *Multifunctional mesoporous silica nanocomposite nanoparticles for theranostic applications*, *Acc. Chem. Res.* **44** (2011) 893.
[8] H. Barrak, T. Saied, P. Chevallier, G. Laroche, A. M'nif and A. H. Hamzaoui, *Synthesis, characterization, and functionalization of zno nanoparticles by n-(trimethoxysilylpropyl) ethylenediamine triacetic acid (tmsedta): Investigation of the interactions between phloroglucinol and zno@ tmsedta*, *Arab. J. Chem.* **12** (2019) 4340.
[9] M. Mansha, A. Qurashi, N. Ullah, F. O. Bakare, I. Khan and Z. H. Yamani, *Synthesis of in2o3/graphene heterostructure and their hydrogen gas sensing properties*, *Ceram. Int.* **42** (2016) 11490.
[10] I. Rawal and A. Kaur, *Synthesis of mesoporous polypyrrole nanowires/nanoparticles for ammonia gas sensing application*, *Sens. Actuator A Phys.* **203** (2013) 92.
[11] I. Khan, Z. H. Yamani, A. Qurashi et al., *Sonochemical-driven ultrafast facile synthesis of sno2 nanoparticles: growth mechanism structural electrical and hydrogen gas sensing properties*, *Ultrason. Sonochem.* **34** (2017) 484.
[12] M. Ganesh, P. Hemalatha, M. M. Peng and H. T. Jang, *One pot synthesized li, zr doped porous silica nanoparticle for low temperature CO_2 adsorption*, *Arab. J. Chem.* **10** (2017) S1501.
[13] M. Shaalan, M. Saleh, M. El-Mahdy and M. El-Matbouli, *Recent progress in applications of nanoparticles in fish medicine: A review*, *Nanomed.: Nanotechnol. Biol. Med.* **12** (2016) 701.
[14] S. Laurent, D. Forge, M. Port, A. Roch, C. Robic, L. Vander Elst et al., *Magnetic iron oxide nanoparticles: synthesis, stabilization, vectorization, physicochemical characterizations, and biological applications*, *Chem. Rev.* **108** (2008) 2064.
[15] N. T. Tien, D. N. Thao, P. T. B. Thao and D. N. Quang, *Key scattering mechanisms limiting the lateral transport in a modulation-doped polar heterojunction*, *J. Appl. Phys.* **119** (2016) 214304.
[16] J. Zhang and M. Saltzman, *Engineering biodegradable nanoparticles for drug and gene delivery*, *Chem. Eng. Prog.* **109** (2013) 25.
[17] S. Gupta, Y. Pathak, M. K. Gupta and S. P. Vyas, *Nanoscale drug delivery strategies for therapy of ovarian cancer: conventional vs targeted*, *Artif. Cells Nanomed. Biotechnol.* **47** (2019) 4066.
[18] S. Kunjachan, J. Ehling, G. Storm, F. Kiessling and T. Lammers, *Noninvasive imaging of nanomedicines and nanotheranostics: principles, progress, and prospects*, *Chem. Rev.* **115** (2015) 10907.
[19] M. Taghavi, M. Tabatabaee, M. H. Ehrampoush, M. T. Ghaneian, M. Afsharnia, A. Alami et al., *Synthesis, characterization and photocatalytic activity of TiO_2/ZnO-supported phosphomolybdic acid nanocomposites*, *J. Mol. Liq.* **249** (2018) 546 .
[20] J. K. Rajput, T. K. Pathak, V. Kumar, H. Swart and L. Purohit, *CdO:ZnO nanocomposite thin films for oxygen gas sensing at low temperature*, *J. Mater. Sci. Eng., B* **228** (2018) 241 .
[21] B. Boro, B. Gogoi, B. Rajbongshi and A. Ramchiary, *Nano-structured TiO_2/ZnO nanocomposite for dye-sensitized solar cells application: A review*, *Renew. Sust. Energ. Rev.* **81** (2018) 2264 .
[22] A. Escobedo-Morales, R. Esparza, A. García-Ruiz, A. Aguilar, E. Rubio-Rosas and R. Pérez, *Structural and vibrational properties of hydrothermally grown ZnO_2 nanoparticles*, *J. Cryst. Growth.* **316** (2011) 37.
[23] L. Román, D. Maurtua, F. Paraguay-Delgado, J. L. Solís and M. M. Gómez, *Green synthesis of ZnO_2 nanoparticles and their annealing transformation into ZnO nanoparticles: Characterization and antimicrobial activity*, *J. Nanosci. Nanotechnol.* **16** (2016) 9889.
[24] A. Kołodziejczak-Radzimska, E. Markiewicz and T. Jesionowski, *Structural characterisation of ZnO particles obtained by the emulsion precipitation method*, *Journal of Nanomaterials* **2012** (2012) .
[25] P. B. Khoza, M. J. Moloto and L. M. Sikhwivhilu, *The effect of solvents, acetone, water, and ethanol, on the morphological and optical properties of ZnO nanoparticles prepared by microwave*, *J. Nanotechnol.* **2012** (2012) 195106.
[26] H. Bai and X. Liu, *Green hydrothermal synthesis and photoluminescence property of ZnO_2 nanoparticles*, *Mater. Lett.* **64** (2010) 341.
[27] N. Uekawa, N. Mochizuki, J. Kajiwara, F. Mori, Y. J. Wu and K. Kakegawa, *Nonstoichiometric properties of zinc oxide nanoparticles prepared by decomposition of zinc peroxide*, *Phys. Chem. Chem. Phys.* **5** (2003) 929.
[28] W. Chen, Y. Lu, M. Wang, L. Kroner, H. Paul, H.-J. Fecht et al., *Synthesis, thermal stability and properties of ZnO_2 nanoparticles*, *J. Phys. Chem. C* **113** (2009) 1320.
[29] M. Egblewogbe, G. Gebreyesus and S. A. Atarah, *Determination of the growth rate of hydrothermally synthesised ZnO_2 crystallites*, *J. Nano Res.* **50** (2017) 41.

[30] C. Bergs, P. Simon, Y. Prots and A. Pich, *Ultrasmall functional ZnO_2 nanoparticles: synthesis, characterization and oxygen release properties*, *RSC Adv.* **6** (2016) 84777.
[31] A. Chatzigoulas, K. Karathanou, D. Dellis and Z. Cournia, *Nanocrystal: A web-based crystallographic tool for the construction of nanoparticles based on their crystal habit*, *J. Chem. Inf. Model* **58** (2018) 2380.
[32] K. Persson, *Materials data on ZnO_2 (sg:205) by materials project*, 7, 2014.
[33] J. Taylor, H. Guo and J. Wang, *Ab initio modeling of quantum transport properties of molecular electronic devices*, *Phys. Rev. B* **63** (2001) 245407.
[34] M. Brandbyge, J.-L. Mozos, P. Ordejón, J. Taylor and K. Stokbro, *Density-functional method for nonequilibrium electron transport*, *Phys. Rev. B* **65** (2002) 165401.
[35] M. Quinten, *Optical properties of nanoparticle systems: Mie and beyond*. John Wiley & Sons, 2010, https://doi.org/10.1002/9783527633135.
[36] D. Singh, S. K. Gupta, Y. Sonvane and I. Lukačević, *Antimonene: a monolayer material for ultraviolet optical nanodevices*, *J. Mater. Chem. C* **4** (2016) 6386.
[37] M. M. Monshi, S. M. Aghaei and I. Calizo, *Band gap opening and optical absorption enhancement in graphene using ZnO nanocluster*, *Phys. Lett. A* **382** (2018) 1171.
[38] M. P. Desjarlais, *Density functional calculations of the reflectivity of shocked xenon with ionization based gap corrections*, *Contrib. to Plasma Phys.* **45** (2005) 300.
[39] J. E. Morales-Mendoza, F. Paraguay-Delgado, J. Moller, G. Herrera-Pérez and N. Pariona, *Structure and optical properties of ZnO and ZnO_2 nanoparticles*, *J. Nano Res.* **56** (2019) 49.